

Photorefractive manipulation of light pulses

B. I. Sturman and E. V. Podivilov

Institute of Automation and Electrometry of Russian Academy of Sciences, 630090 Novosibirsk, Russia

M. V. Gorkunov

Institute of Crystallography of Russian Academy of Sciences, 119333 Moscow, Russia

(Received 11 February 2008; published 9 June 2008)

We investigate theoretically the main elements of manipulation of light pulses—strong nonlinear slowing down, trapping, and release on demand—in photorefractive nonlinear media. This includes a study of the slowing-down characteristics, such as delay time, amplification factor, and nonlinear broadening, for different types of photorefractive response and interaction geometries, as well as an analysis of the shape of pulses released after a long storage. The photorefractive manipulation method is shown to be applicable at ambient temperatures, low light intensities, and wide spectral ranges.

DOI: [10.1103/PhysRevA.77.063808](https://doi.org/10.1103/PhysRevA.77.063808)

PACS number(s): 42.65.Hw, 42.50.Gy, 78.20.Bh

I. INTRODUCTION

The current burst of research interest in light slowing down is centered predominantly on nonlinear mechanisms of this fundamental phenomenon [1–5]. It is well understood nowadays that nonlinear techniques allow reduction of the effective velocities of light pulses by many orders of magnitude, which exceeds the known capabilities of the linear schemes [6]. Apart from an obvious fundamental interest, the slowing-down phenomenon is promising for various applications, including development of sensitive detectors and delay lines and, potentially, quantum-information processing [4,7].

One of the most impressive examples of pulse deceleration (velocity of ≈ 17 m/s) occurs in the resonant nonlinearity of ultracold gases [8]; it is closely related to the quantum effect of electromagnetically induced transparency (EIT) [9]. Moreover, the EIT-based nonlinear schemes have allowed also for long-term trapping of light pulses in the form of atomic coherence with their subsequent release on demand [10].

The drawbacks of the EIT-based technique are ultralow temperatures, very narrow resonances, and the necessity to use high light intensities. For practical purposes, the use of ambient temperatures, solid state nonlinear materials, and common light sources has no real alternative. This is why numerous attempts to employ room-temperature resonant nonlinearities of solids have been undertaken; see [3,11–14] and references therein. The achieved slowing-down characteristics are still modest and related mostly to periodically modulated signals, while high light intensities are still required.

Recently, photorefractive (PR) nonlinearity was employed for deceleration of light pulses [15–18] and propagation velocities lower than 0.025 cm/s were reported [15]. PR nonlinearity possesses numerous advantages for light slowing down. No sharp frequency adjustment is needed, operation at room temperature with continuous-wave lasers is ensured, many PR materials are available, and achievement of a high-level nonlinearity is not difficult [19,20]. Moreover, the PR nonlinearity offers excellent possibilities for long-term trapping and the subsequent release of light pulses: The refractive index changes are caused by the light-induced space-

charge fields and the decay time of these fields in the dark can be huge.

In this paper, we investigate theoretically the capabilities of the PR nonlinearity for manipulating light pulses. We deal first with slowing-down characteristics. The time delay, the output pulse width, and the peak amplification factor are investigated as functions of the coupling strength and the input width for two distinct types of PR response, the local and nonlocal, and two different interaction geometries. The effects of pump depletion are taken into account. We analyze then the trapping of light pulses and their subsequent release on demand, after long-term storage, for the simplest type of PR nonlinearity—the nonlocal response. This includes calculations of the stored space-charge field profiles for different values of the trapping time (the time of pump interruption) and an analysis of the shape of the released pulses. Finally, we discuss the main advantages and drawbacks of the photorefractive technique in question.

II. THEORETICAL BACKGROUND

We restrict ourselves to the most common transmission (T) and reflection (R) two-wave coupling geometries depicted in Figs. 1(a) and 1(b). In both cases, we have a permanent pump wave and a pulse-shaped signal wave at the input. The propagation coordinate z ranges from 0 to the crystal thickness d . The carrier frequency of the waves is expected to be the same; we are dealing thus with an almost frequency-degenerate two-wave coupling. The light absorption is supposed to be negligible.

The slowly varying complex amplitudes of the signal and pump waves, $A=A(z,t)$ and $A_p=A_p(z,t)$, obey the known coupled-wave equations that follow from the Maxwell equations [20,21]:

$$\frac{\partial A}{\partial z} = -i\kappa E_K A_p, \quad (1)$$

$$\frac{\partial A_p}{\partial z} = \mp i\kappa E_K^* A, \quad (2)$$

where the upper and lower signs in Eq. (2) correspond to the transmission and reflection cases, respectively, $E_K=E_K(z,t)$

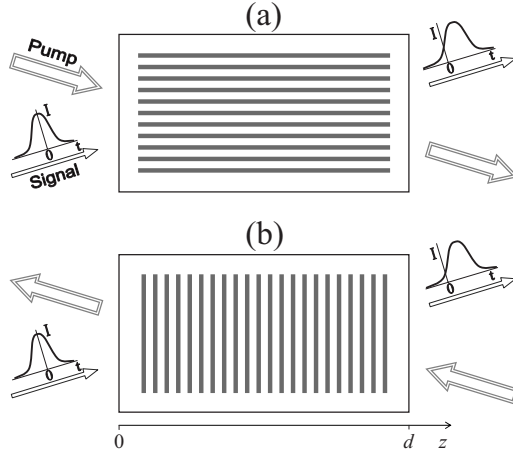


FIG. 1. Two main geometries, transmission (a) and reflection (b), for the PR deceleration of light pulses. The parallel lines represent the grating fringes.

is the amplitude of the space-charge field (the grating amplitude) at the difference spatial frequency of the light waves, K , $\kappa = \pi n^3 r / \lambda$, n is the background refractive index, r is the relevant electro-optic coefficient, λ is the light wavelength, and the asterisk indicates complex conjugation. The squared absolute values $I = |A|^2$ and $I_p = |A_p|^2$ will be referred to as the intensities of the signal and pump waves, respectively. As follows from Eqs. (1) and (2), we have $\partial(I \pm I_p) / \partial z = 0$; this relation expresses the energy conservation law for the light waves.

The simplest and highly useful material equation for the grating amplitude has the form [20,21]

$$\left(t_r \frac{\partial}{\partial t} + 1 \right) E_K = \frac{E_s A A_p^*}{|A|^2 + |A_p|^2}, \quad (3)$$

where t_r is the response time, and E_s is the characteristic electric field. The combination of light amplitudes in the right-hand side is the half contrast of the light-interference pattern. The response time can often be identified with the dielectric relaxation time, $t_r \approx \epsilon \epsilon_0 / \sigma$, where $\epsilon \epsilon_0$ is the static dielectric constant and σ is the spatially averaged conductivity. With the light on, the dark conductivity is typically negligible compared to the photoconductivity. In this case, we have $t_r \propto (|A|^2 + |A_p|^2)^{-1}$; in continuous-wave experiments it ranges roughly from 10^{-3} to 10^2 s. With the light off, the time t_r is determined by the dark conductivity; the relaxation can last here for hours, days, or even years.

The characteristic field E_s entering Eq. (3) is generally a complex quantity. The limiting cases of real and imaginary E_s are referred to as the cases of local and nonlocal PR response, respectively [20,22]. For the local response, the steady-state index grating is not shifted (or is π shifted) with respect to the light intensity grating. This response can be attributed to the dominating drift or photovoltaic charge transport, and E_s can be equalized to the applied field E_0 or to the photovoltaic field E_{pv} . The latter can be as high as $(10^4 - 10^5)$ V/cm in LiNbO_3 and LiTaO_3 crystals [23,24]. For the nonlocal response, the index grating is $\pi/2$ shifted with respect to the light pattern. This case occurs when the

diffusion of the photoexcited electrons (or holes) is the main charge-transport mechanism. Here we have $E_s = iE_D$, where $E_D = K k_B T / e$ is the diffusion field, T is the absolute temperature, k_B is Boltzmann's constant, and e is the elementary charge. Typically, $E_D \lesssim 10^3$ and $\sim 10^4$ V/cm for the transmission and reflection geometries. The effects of spatial dispersion, including the Debye screening, can diminish E_s and affect t_r for sufficiently large values of the spatial frequency K , which is especially important for the reflection geometry [20].

When the signal wave is relatively weak, $|A|^2 \ll |A_p|^2$, the undepleted pump approximation is applicable. In this case, $A_p \approx \text{const}$ and Eqs. (1)–(3) transform to the set of linear differential equations for the normalized amplitudes $a = A/A_p$ and $u = E_K/E_s$:

$$\frac{\partial a}{\partial z} = \gamma_0 u, \quad (4)$$

$$\left(t_r \frac{\partial}{\partial t} + 1 \right) u = a, \quad (5)$$

where $\gamma_0 = -i\kappa E_s \equiv -i\pi n_0^3 r E_s / \lambda$ is the so-called coupling coefficient. It is generally a complex quantity which characterizes the type and strength of the PR response. The undepleted pump approximation plays an important role in our theory. Within this approximation and for the same input parameters there is no difference between the transmission and reflection cases.

Employing the Fourier transformation in time, $a(z, t) \rightarrow a_\omega(z)$, we come from the set (4) and (5) to the following explicit single expression for $a_\omega(z)$:

$$a_\omega(z) = a_\omega(0) \exp(g_\omega z), \quad (6)$$

where $a_\omega(0)$ is the input value of $a_\omega(z)$ and

$$g_\omega = \frac{\gamma_0}{1 - i\omega t_r} \quad (7)$$

is the rate of spatial changes for the ω component of the input signal. Its real part g'_ω is apparently the rate of spatial amplification, while the imaginary part g''_ω is the nonlinear correction to the z component of the wave vector of the signal wave. This part can be attributed to the effective group velocity $v_g(\omega) = (dg''_\omega/d\omega)^{-1}$.

As is clear already from Eqs. (6) and (7), the strength of the nonlinear effects can generally be characterized by the dimensionless parameter $|\gamma_0|d$; in what follows it is referred to as the coupling strength. The most important effects occur in the range $|\gamma_0|d \gtrsim 1$ where the frequency-dependent spatial amplification is indispensable and the group velocity $v_g(\omega)$ is insufficient for characterization of the pulse propagation.

It is worthy of mention that the simplest material equation (3) admits important generalizations. First, the relaxation rate t_r^{-1} can be a complex quantity with a relatively large imaginary part [20,26]. This is, in particular, the case of cubic crystals of the sillenite family, $\text{Bi}_{12}\text{SiO}_{20}$, $\text{Bi}_{12}\text{TiO}_{20}$, and $\text{Bi}_{12}\text{GeO}_{20}$. Second, the PR response must sometimes be characterized by a higher-order differential operator in the left-hand side of Eq. (3). Such a situation occurs, e.g., in

ferroelectric $\text{Sn}_2\text{P}_2\text{S}_6$ [27,28]. The mentioned generalizations can be easily incorporated into our theory: Eq. (6) remains unchanged while the particular form of the frequency dependence g_ω is modified. In this paper, we restrict ourselves to the simplest type of frequency dependence given by Eq. (7).

Using Eq. (6), we can analyze the shape of the output pulse for different types of PR response and different input signals. It is essential that the dependence g_ω is resonantlike; for $|\omega|t_r \gg 1$ the rate coefficient is very small. The width of the resonance is given by the inverse response time t_r^{-1} . Furthermore, it is worthy of notice that the right-hand side of Eq. (6) depends *exponentially* on the product $\gamma_0 z$; for $\gamma_0 d \gg 1$ one can expect a strong impact of the type and strength of the PR response on the output pulse characteristics.

III. SLOWING-DOWN CHARACTERISTICS

A. Nonlocal response

In this simplest case, the coupling coefficient γ_0 is real. The amplification coefficient $g'_\omega = \gamma_0 / (1 + \omega^2 t_r^2)$ is here an even function of the frequency which peaks at $\omega = 0$, whereas the wave vector correction $g''_\omega = \gamma_0 \omega t_r / (1 + \omega^2 t_r^2)$ is an odd function of ω . Correspondingly, the introduced effective group velocity v_g is an even function of ω . The maximum value of g'_ω is twice larger than that of $|g''_\omega|$ so that the effects of spatial amplification are expected to be stronger than the dispersive effects.

Many important features of the pulse deceleration can be described within the undepleted pump approximation. To determine the output shape of the pulse, we need to specify the input amplitude $A(0, t)$. The Gaussian input shape $A(0, t) = A_0 \exp(-t^2/t_0^2)$ with t_0 being the width parameter is useful for analytical and numerical treatments. The input half-width, taken at the half-height of $I(0, t)$, is here $w_0 = \sqrt{\ln 2} t_0$. The normalized output amplitude $A(d, t)/A_0$ is given by

$$\frac{A(d, t)}{A_0} = \frac{t_0}{\sqrt{\pi} t_r} \int_0^\infty \exp\left(\frac{\gamma_0 d}{1+s^2} - \frac{s^2 t_0^2}{4t_r^2}\right) \cos\left[s\left(\frac{t}{t_r} - \frac{\gamma_0 d}{1+s^2}\right)\right] ds, \quad (8)$$

which is a real quantity. Both amplification and dispersive effects contribute to the right-hand side. The dependence of $A(d)/A_0$ on the normalized time t/t_r is controlled by two dimensionless parameters, the so-called coupling strength $\gamma_0 d$ and the ratio t_0/t_r . Similarly, one can characterize $A(d, t)$ for any other particular input shape, e.g., for the Lorentz one, $A(0, t) = A_0 / (1 + t^2/t_0^2)$. Except for quantitative details, the output characteristics are the same for the Gaussian and Lorentzian input pulses.

The left column in Fig. 2, curves (a) to (d), shows the output intensity profile for $t_0/t_r = 3$ and four incrementally increasing values of the coupling strength. Curve (a) corresponds to $\gamma_0 d = 0$ (the input intensity profile), whereas curves (b), (c), and (d) are plotted for $\gamma_0 d = 3, 6,$ and 9 , respectively, using Eq. (8). Clearly, we have a single output pulse which is significantly delayed. The delay time Δt , defined as the time of maximum of $I(d, t)$, increases almost linearly with $\gamma_0 d$. Furthermore, the output pulse experiences a noticeable non-

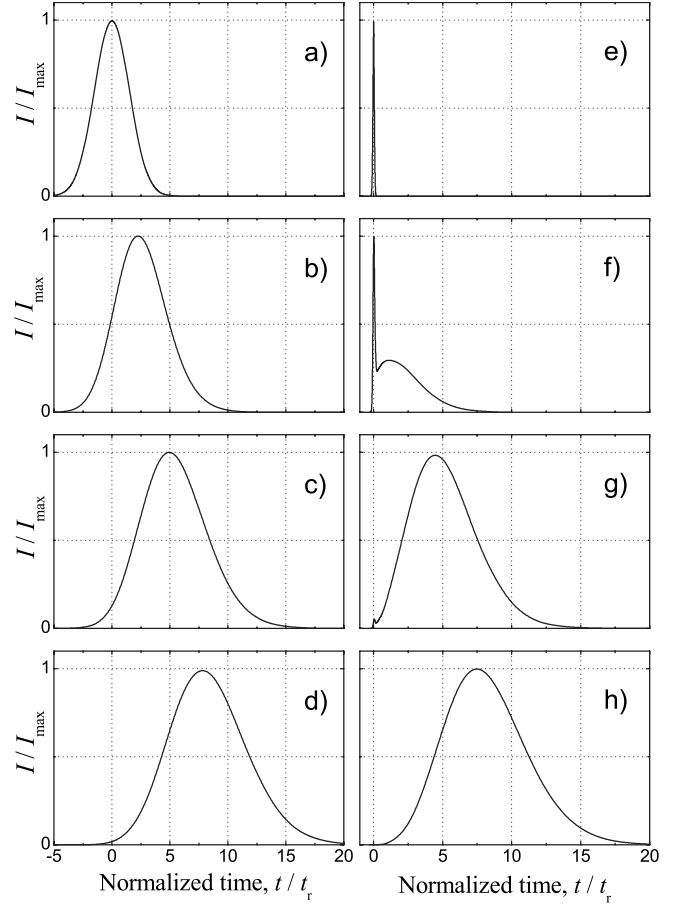


FIG. 2. The normalized output intensity profile $I(d, t)/I_{\max}$ versus the normalized time t/t_r . The left and right columns correspond to $t_0/t_r = 3$ and 0.1 , respectively. The curves of the first, second, third, and fourth rows are plotted for $\gamma_0 d = 0$ (the input profiles), $3, 6,$ and 9 , respectively.

linear broadening; the output temporal width grows with $\gamma_0 d$. For the largest value of $\gamma_0 d$, the effect of time delay clearly dominates over the broadening. Last, the output pulses are amplified. The peak amplification factor I_{\max}/I_0 , where $I_0 = |A_0|^2$ and $I_{\max} = [I(d, t)]_{\max}$, is approximately $2.43 \times 10^2, 6.7 \times 10^4,$ and 2.1×10^7 for the cases (b), (c), and (d), respectively.

For sufficiently short input pulses, the shape transformations are essentially different (see also [15]). The right column in Fig. 2, curves (e) to (h), shows what happens with increasing coupling strength for $t_0/t_r = 0.1$. For $\gamma_0 d = 3$, the output intensity profile $I(d, t)$ possesses two maxima, the main practically unshifted narrow peak and a broad shifted maximum at $\Delta t/t_r \approx 1.5$. For $\gamma_0 d = 6$ the two-maxima structure survives, but the broad maximum at $\Delta t/t_r \approx 4.5$ becomes dominant. For $\gamma_0 d = 9$ we have a single peak whose position and width are not much different from those for $t_0/t_r = 3$; compare curves (d) and (h). The peak amplification factors for the cases (f), (g), and (h) are approximately $1.7, 0.8 \times 10^2,$ and 2×10^4 . They are much smaller than the amplification factors for the cases (b), (c), and (d), respectively.

Generally, there are two regions (1 and 2) on the plane of the input parameters $\gamma_0 d$ and t_0/t_r where the output pulse

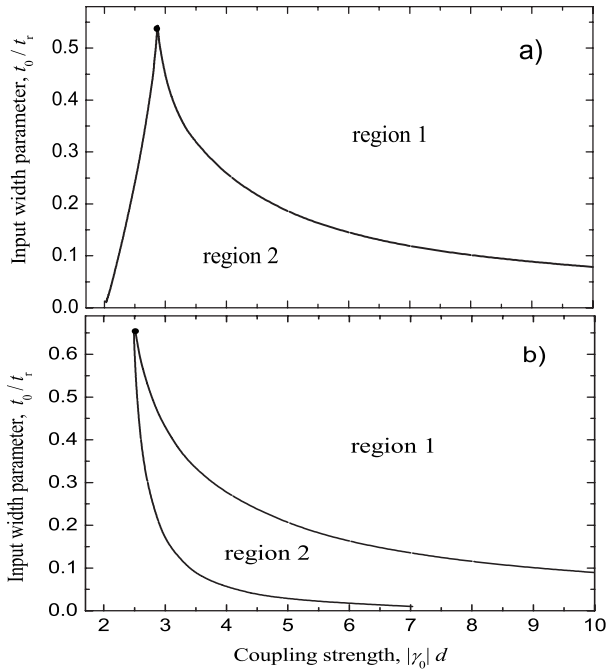


FIG. 3. Line separating the regions 1 and 2 where the output intensity profile $I(t)$ possesses a single maximum and two maxima, respectively, for the nonlocal (a) and local (b) nonlinear responses. The critical (kink) point $(\gamma_0 d)_c, (t_0/t_r)_c$, marked by a dot, is 2.87, 0.55 and 2.5, 0.6656 for these cases.

possesses one maximum and two maxima. The curve separating these regions is shown in Fig. 3(a). For $t_0/t_r > 0.533$ the output intensity profile always possesses a single maximum. The narrow unshifted peak is dominating only in the vicinity of the left border of the region 2.

The physics of the pulse delay and amplification can be explained in terms of photorefractive two-wave coupling [20]. The energy transfer from the pump to the signal wave is due to the inertial processes of recording and erasure of the index grating and instantaneous Bragg diffraction from this grating. In the case of nonlocal response, the index grating is $\pi/2$ shifted with respect to the light interference fringes. This circumstance facilitates diffraction from the pump to the signal wave, which increases the light contrast and accelerates the recording process in the depth of the crystal. For $\gamma_0 d \gg 1$, this process of self-enhancement [29] (diffraction \rightarrow rerecording \rightarrow diffraction...) persists for $t \gg t_r$ even in the absence of the input signal wave, and the index grating becomes more and more localized near the output face of the crystal, disappearing finally near this face. In accordance with this interpretation, short input pulses produce merely a weak seed grating which develops then in the presence of the pump. In any case, the pulse delay ($\Delta t > 0$) is rooted in the inertial nature of the PR nonlinearity.

Consider now the main intensity-related output parameters—the normalized delay time $\Delta t/t_r$, the normalized output half-width w/t_r , and the peak amplification factor I_{\max}/I_0 —as functions of the input width parameter t_0/t_r for several representative values of the coupling strength $\gamma_0 d$. The corresponding numerical results are presented in Fig. 4 for $t_0/t_r \geq 0.1$. The normalized time delay $\Delta t/t_r$ grows rather

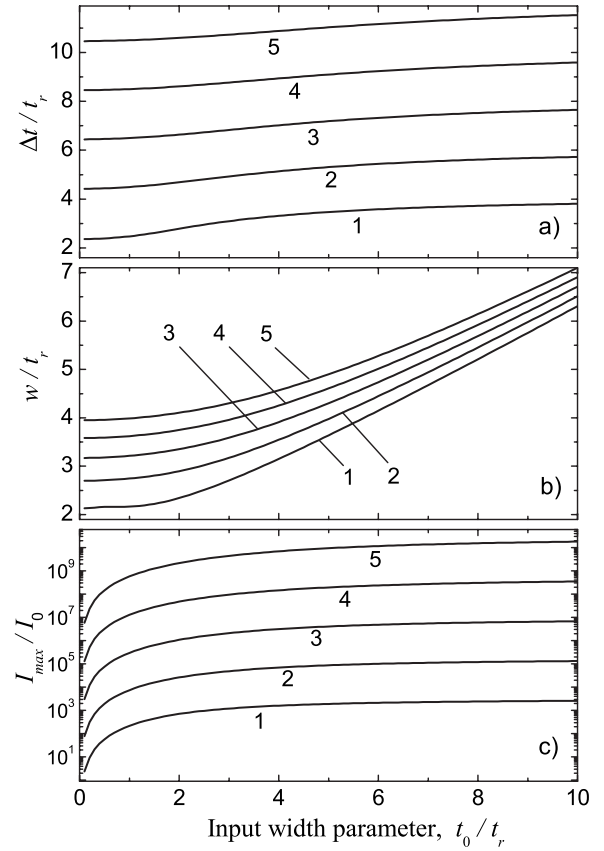


FIG. 4. The output parameters $\Delta t/t_r$ (a), w/t_r (b), and $I_{\max}(d,t)/I_0$ (c) versus the normalized input width parameter t_0/t_r . Curves 1, 2, 3, 4, and 5 correspond to $\gamma_0 d = 4, 6, 8, 10$, and 12, respectively.

slowly with t_0/t_r and almost linearly with $\gamma_0 d$. For $\gamma_0 d \gg 1$ it can be estimated from the relation $\Delta t/t_r \approx \gamma_0 d$. The behavior of the output half-width parameter w/t_r is different. It grows significantly with both t_0/t_r and $\gamma_0 d$. For $t_0/t_r \gg (\gamma_0 d)^{1/2}$ the nonlinear broadening is relatively weak and $w \approx w_0 \equiv \sqrt{\ln 2}/2t_0$. In the opposite limit it is dominant; we have here $w \gg w_0$ and $w/t_r \approx (\gamma_0 d)^{1/2}$. The peak amplification factor I_{\max}/I_0 first grows sharply with t_0/t_r and then saturates on the steady-state level given by $\exp(2\gamma_0 d)$. For $t_0/t_r \ll 1$ and $\gamma_0 d \gg 1$ the amplification factor is given by $I_{\max}/I_0 \approx (t_0/t_r)^2 (2\gamma_0 d)^{-1} \exp(2\gamma_0 d)$. The above approximate analytical expressions are obtained by the saddle-point method [25].

Two different requirements to the output pulse parameters have to be distinguished. The strongest requirement is for a large pulse delay combined with minor shape changes, which is expressed by $\Delta t \gg w_0$, $w \approx w_0$. In accordance with our analysis, it is satisfied for $t_0/t_r \ll \gamma_0 d \ll t_0^2/t_r^2$, i.e., broad input pulses and very large values of the coupling strength. Achievement of such values of $\gamma_0 d$ does not present fundamental difficulties, but it can lead to unwanted nonlinear noise or losses in the form of light-induced scattering [20]. The second (softer) requirement is merely the inequality $\Delta t \gg w$; it is satisfied for $t_0/t_r \ll 1$ and $\gamma_0 d \gg 1$ when the shape changes are strong but the spatial amplification is not yet strong enough to provoke the light-induced noise.

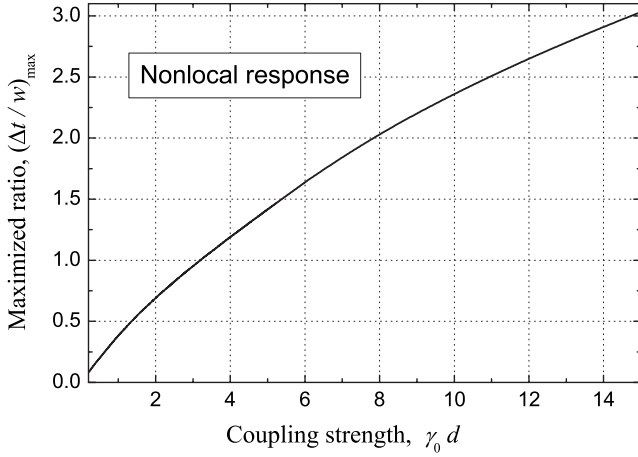


FIG. 5. The maximum (in t_0/t_r) value of the ratio $\Delta t/w$ versus the coupling strength for the nonlocal response.

Figure 5 shows the ratio $(\Delta t/w)_{\max}$, maximized in t_0/t_r , as a function of the coupling strength. It expresses the capability of the nonlocal response for strong deceleration of light pulses. The values of $\Delta t/w$ which are very close to $(\Delta t/w)_{\max}$ can be achieved under a soft restriction on the input width parameter, $t_0/t_r \ll 1$. At the same time, the amplification factor I_{\max}/I_0 can be made not too large by decreasing t_0/t_r ; see Figs. 3 and 4 for more details.

B. Effect of pump depletion

Beyond the undepleted pump approximation, the output pulse characteristics are different for the transmission and reflection configurations of Fig. 1. The main question is whether the pump depletion can improve the output characteristics. It is unlikely for the transmission case because the pump amplitude A_p decreases with increasing propagation coordinate z deteriorating thus the basic self-enhancement process. In the reflection case, the situation is more complicated. Pump depletion results here in increasing the amplitude $A_p(z)$. This facilitates the long-term nonlinear dynamics and leads to increase in both the time delay and the output width. Which of these effects is dominating is far from evident.

To analyze the effect of pump depletion, we employed Eqs. (1)–(3) with $E_s = i|E_s|$. The boundary condition for the signal wave, $A(0, t) = A_0 \exp(-t^2/t_0^2)$, corresponds again to a Gaussian input pulse; the boundary condition for the pump wave is $A_p(0, t) = A_p^0 = \text{const}$ for the transmission case and $A_p(d, t) = A_p^0 = \text{const}$ for the reflection case; see Fig. 1. The intensity ratio $I_0/I_p^{\text{in}} = |A_0/A_p^0|^2$ is a variable parameter.

The numerical procedure was strongly simplified by the introduction of the dimensionless variable $\xi = \xi(z, t)$, such that

$$\xi(z, t) = \gamma_0 \int_0^z u(z', t) dz', \quad (9)$$

where, as earlier, $u = E_K/E_s$ is the normalized grating amplitude. The light amplitudes can be expressed then by ξ using Eqs. (1) and (2). The corresponding explicit relations are

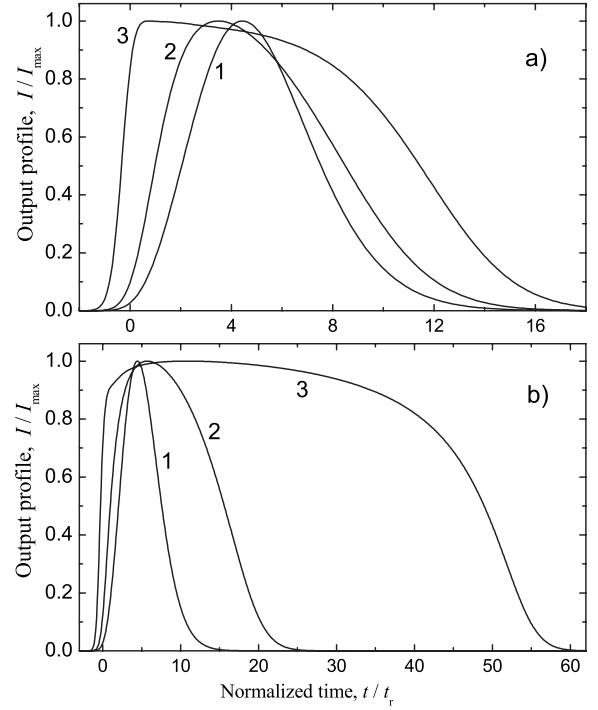


FIG. 6. The impact of pump depletion on the shape of the output pulse for the transmission (a) and reflection (b) geometries. Curves 1 correspond to the undepleted pump regime, while curves 2 and 3 are plotted for the input intensity ratio $I_0/I_p^{\text{in}} = 4 \cdot 10^{-4}$ and 10^{-6} , respectively. The coupling strength is $\gamma_0 d = 6$. Note the difference in the time scales in a) and b).

$$\frac{A}{A_p} = a_0 \cosh \xi + \sinh \xi, \quad \frac{A_p}{A_p^0} = \cosh \xi + a_0 \sinh \xi \quad (10)$$

for the transmission case and

$$\frac{A}{A_p^0} = a_0 \cos \xi + \nu \sin \xi, \quad \frac{A_p}{A_p^0} = \nu \cos \xi - a_0 \sin \xi \quad (11)$$

for the reflection case, where $a_0(t) = A(0, t)/A_p^0$ is the normalized amplitude of the input signal and $\nu(t) = [1 + a_0 \sin \xi(d, t)] / \cos \xi(d, t)$. The boundary conditions for the light amplitudes are satisfied automatically. Substituting Eqs. (10) and (11) into Eq. (3), we come to a single nonlinear equation for $u(z, t)$.

Figure 6(a) shows representative numerical data for the transmission geometry, $\gamma_0 d = 6$, and $t_0/t_r = 1$. Curve 1 is plotted within the undepleted pump approximation, while curves 2 and 3 are calculated from Eqs. (1)–(3) for $I_0/I_p^{\text{in}} = 10^{-6}$ and 4×10^{-3} , respectively. The pump depletion is noticeable for curve 2 and strong for curve 3. It leads, as expected, to decreasing time delay Δt . To avoid strong pump depletion, the input intensity ratio I_p^{in}/I_0 must be larger than the intensity amplification factor within the undepleted pump approximation; see above.

Curves 1–3 in Fig. 6(b) are plotted for the reflection geometry and the same input parameters. The influence of the pump depletion is essentially different. It results in increasing both the time delay Δt and the output half-width w . Fur-

thermore, pump depletion leads to strong flattening of the pulse top. The ratio $\Delta t/w$, which is an important figure of merit for pulse deceleration, is decreasing because of the pump depletion.

C. Local response

The coupling constant γ_0 is purely imaginary here; without loss of generality it can be represented as $\gamma_0 = -i|\gamma_0|$. In contrast to the case of nonlocal response, the amplification coefficient $g'_\omega = |\gamma_0|\omega t_r / (1 + \omega^2 t_r^2)$ and the wave vector correction $g''_\omega = -|\gamma_0| / (1 + \omega^2 t_r^2)$ are odd and even functions of ω , respectively. The steady-state ($\omega=0$) amplification is absent and the maximum value of the amplification coefficient g'_ω is twice smaller than that of $|g''_\omega|$. In other words, the dispersive effects are expected to be more pronounced in this case.

Within the undepleted pump approximation and for the accepted Gaussian shape of the input pulse, we have for the normalized output amplitude $A(d, t)/A_0$

$$\frac{A(d, t)}{A_0} = \frac{t_0}{\sqrt{\pi} t_r} \int_0^\infty \exp(-s^2 t_0^2 / 4 t_r^2) (F'_s - i F''_s) ds, \quad (12)$$

where the functions of the integration variable F'_s and F''_s are given by

$$\begin{aligned} F'_s &= \cos\left(\frac{|\gamma_0|d}{1+s^2}\right) \cosh\left(\frac{s|\gamma_0|d}{1+s^2}\right) \cos(st) \\ &\quad - \sin\left(\frac{|\gamma_0|d}{1+s^2}\right) \sinh\left(\frac{s|\gamma_0|d}{1+s^2}\right) \sin(st), \\ F''_s &= \cos\left(\frac{|\gamma_0|d}{1+s^2}\right) \sinh\left(\frac{s|\gamma_0|d}{1+s^2}\right) \sin(st) \\ &\quad + \sin\left(\frac{|\gamma_0|d}{1+s^2}\right) \cosh\left(\frac{s|\gamma_0|d}{1+s^2}\right) \cos(st). \end{aligned} \quad (13)$$

As earlier, both g'_ω and g''_ω influence the shape of the output pulse, and again this shape is controlled by two dimensionless parameters, the input width parameter t_0/t_r and the coupling strength $|\gamma_0|d$. However, the ratio $A(d, t)/A_0$ is a complex quantity.

In many respects, the behavior of the output pulses versus the control parameters is similar to that for the nonlocal response. The pulses experience time delay, broadening, and spatial amplification. The delay time Δt , the output half-width w , and the peak amplification factor I_{\max}/I_0 grow again with increasing coupling strength. Furthermore, we have again the two-maxima regime for sufficiently narrow input pulses. Qualitatively, these features are not much different from those illustrated by Fig. 2. However, there are important differences—qualitative and quantitative. Consider now the output characteristics in more detail.

Figure 3(b) shows the line separating the single-maximum and two-maxima regions on the plane of the input parameters $|\gamma_0|d$ and t_0/t_r . It differs essentially from the separatrix of Fig. 3(a). The critical value of the input width parameter is $(t_0/t_r)_c \approx 0.6656$; for $t_0/t_r > (t_0/t_r)_c$ the output pulse always has a single maximum. The critical value of the coupling

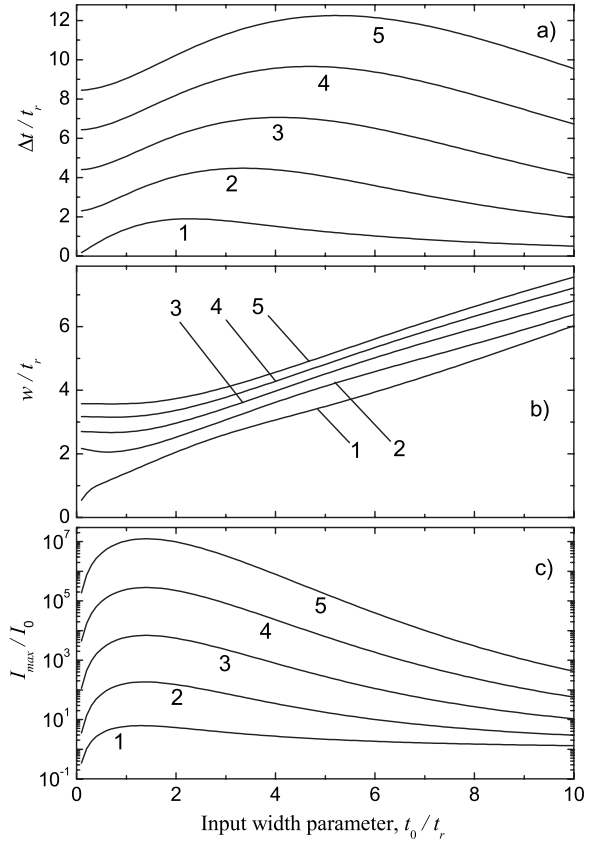


FIG. 7. Dependences of $\Delta t/t_r$ (a), w/t_r (b), and I_{\max}/I_0 (c) on t_0/t_r for the local response. Lines 1, 2, 3, 4, and 5 are plotted for $|\gamma_0|d = 4, 8, 12, 16,$ and 20 , respectively.

strength is $(|\gamma_0|d)_c \approx 2.5$. For $|\gamma_0|d < (|\gamma_0|d)_c$, the output pulse always has a single maximum and the peak amplification factor I_{\max}/I_0 is modest. For $|\gamma_0|d \gg (|\gamma_0|d)_c$, the narrow unshifted peak of $I(d, t)$ becomes important only for very small values of t_0/t_r near the lowest branch of the separatrix; otherwise, the broad shifted maximum is dominant.

Figure 7 shows the main output parameters versus t_0/t_r for several representative values of $|\gamma_0|d$. Both the time delay and the amplification factor grow initially with this variable and then decrease. This feature is new (compare to Fig. 4), but it is not surprising because the steady-state ($t_0/t_r \rightarrow \infty$) spatial amplification is not possible for the local response. At the same time, the positions of the maxima of $\Delta t/t_r$ and I_{\max}/I_0 are essentially different for the same $|\gamma_0|d$. This evidences that the dispersive effects (caused by g''_ω) play an important role in the nonlinear pulse propagation. As is clear from Fig. 7(b), the ratio w/t_r is a growing function of t_0/t_r , except for the initial section $t_0/t_r \lesssim 1$ for intermediate values of $|\gamma_0|d$ where curves 2 and 3 possess shallow minima.

Comparing Fig. 7(a) with Fig. 4(a), we see that the normalized time delay $\Delta t/t_r$ (as well as w/t_r and I_{\max}/I_0), taken at the same combination of input parameters, is generally smaller for the local response. This is indeed due to the fact that the effects of spatial amplification are relatively weak here. One might suggest on these grounds that the local response is less efficient for the purposes of pulse deceleration. However, this is not quite true. The point is that the attain-

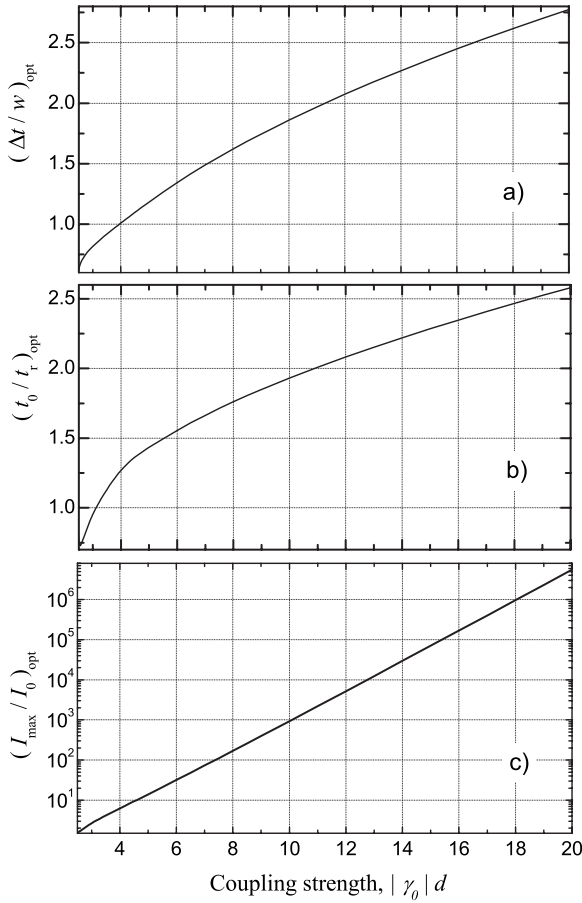


FIG. 8. Dependences of the optimum values of $\Delta t/w$ (a), t_0/t_r (b), and I_{max}/I_0 (c) on the coupling strength for the local response.

able values of the coupling strength $|\gamma_0|d$ are typically larger than the values of $\gamma_0 d$ for the nonlocal response. For the pulse deceleration, it is important to achieve large values of the ratio $\Delta t/w$ with modest peak amplification factors to avoid nonlinear noise in the form of light-induced scattering.

The behavior of the curves in Figs. 7(a) and 7(b) suggests a simple optimization scheme: The ratio $\Delta t/w$ possesses, as a function of t_0/t_r , a well-pronounced maximum. Its position $(t_0/t_r)_{\text{opt}}$ and the corresponding values $(\Delta t/w)_{\text{opt}}$ and $(I_{\text{max}}/I_0)_{\text{opt}}$ depend only on the coupling strength. These dependences give important predictions and allow a judgment about the capabilities of the local response for pulse deceleration. They are presented in Fig. 8. One sees that values $\Delta t/w > 2$ can be achieved here for $|\gamma_0|d \approx 12$ and $I_{\text{max}}/I_0 < 10^4$; the nonlinear broadening remains not very strong here, $w/w_0 \approx 2$. For the nonlocal response, the above combination of output parameters would not be possible at the same level of spatial amplification.

Apart from the above optimization scheme, which maximizes $\Delta t/w$ in t_0/t_r , leads to quite large values of I_{max}/I_0 , and is specific for the local response, we can consider also the case of narrow input pulses, $t_0/t_r \ll 1$, and large values of the coupling strength, $|\gamma_0|d \gg 1$, when we are not far from the upper branch of the separatrix of Fig. 3(b).

As one can see from Fig. 7, the ratio $\Delta t/w$ is not much smaller here than $(\Delta t/w)_{\text{opt}}$, but the peak amplification factor

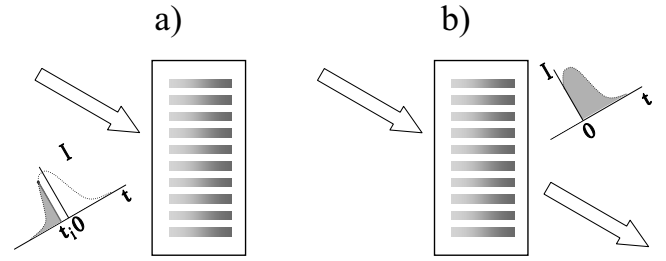


FIG. 9. Sequence of operations for trapping (a) and release (b) of light pulses for the T geometry.

I_{max}/I_0 is much smaller than $(I_{\text{max}}/I_0)_{\text{opt}}$. As in the case of nonlocal response, modest amplification factors are obtained here at the expense of strong nonlinear distortions, $w/w_0 \gg 1$.

The influence of pump depletion on the output characteristics is similar to that for the case of nonlocal response; it is always negative and should be avoided.

IV. TRAPPING, STORAGE, AND RELEASE OF LIGHT PULSES

The problem to be considered can be formulated as follows: Let us *interrupt* the pump and signal (or the pump alone) at an arbitrary moment of time t_i [see Fig. 9(a)]. Then the photoconductivity drops by several orders of magnitude, the space-charge grating recorded up to this moment becomes frozen, and the pulse can be viewed as trapped (stopped). The storage time of the frozen space-charge field (of the trapped pulse) is limited from above by the dielectric relaxation time t_d caused by the dark conductivity. This time can be as long as hours, days, and even years in photorefractive materials such as BaTiO₃ and LiNbO₃ crystals [20].

Imagine now that the pump is switched on again after a long storage time [see Fig. 9(b)]. The pump beam experiences Bragg diffraction from the grating into the signal beam and eventually erases this grating. The problems to consider are as follows: What is the shape of the outgoing pulse? How does this shape depend on the interruption time t_i and other parameters? Is it possible to restore the initial pulse shape during such a release? Below we analyze these problems for the simplest case of nonlocal response within the undepleted pump approximation. While we refer for definiteness to the transmission geometry, the subsequent results are equally applicable to the reflection case.

Turning to the description of the above manipulation steps, we adopt normalized or dimensionless variables. In addition to the above introduced normalized grating and light amplitudes, $u = E_K/E_s$ and $a = A/A_p$, we define also the normalized time $\tilde{t} = t/t_r$, the normalized input width $\tilde{t}_0 = t_0/t_r$, the normalized interruption time $\tilde{t}_i = t_i/t_r$, the dimensionless propagation coordinate $\tilde{z} = \gamma_0 z$, and the dimensionless crystal thickness $\tilde{d} = \gamma_0 d$.

As the first step of our description, we calculate the recorded or frozen field profile $u_i = u(\tilde{z}, \tilde{t}_i)$. Using the Fourier transformation, it is easy to find from Eqs. (4) and (5) for the Gaussian input signal that

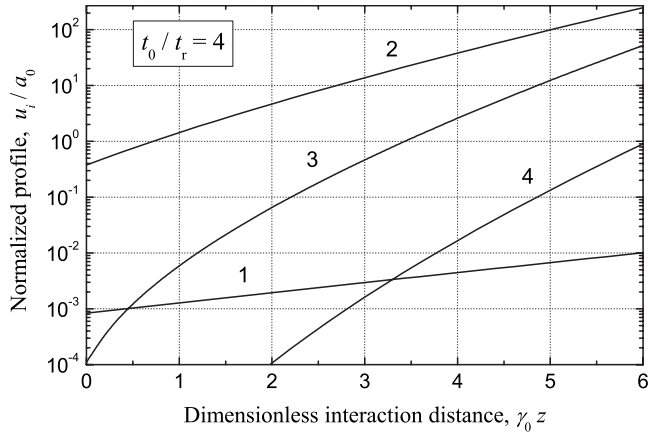


FIG. 10. The normalized grating amplitude u_i versus the dimensionless propagation coordinate $\gamma_0 z$ for $t_0/t_r=4$ and different values of the interruption time t_i . Curves 1, 2, 3, and 4 correspond to $t_i/t_r=-10, 5, 15,$ and $25,$ respectively.

$$\frac{u_i}{a_0} = \frac{\tilde{t}_0}{\sqrt{\pi}} \int_0^\infty \exp\left(\frac{\tilde{z}}{1+s^2} - \frac{s^2 \tilde{t}_0^2}{4}\right) \left\{ \cos\left[s\left(\tilde{t}_i - \frac{\tilde{z}}{1+s^2}\right)\right] + s \sin\left[s\left(\tilde{t}_i - \frac{\tilde{z}}{1+s^2}\right)\right] \right\} \frac{ds}{1+s^2}, \quad (14)$$

where $a_0=A_0/A_p$. The right-hand side of this relation is real. Since the characteristic field E_s is imaginary for the nonlocal response, this means that the grating amplitude E_K remains purely imaginary (a $\pi/2$ -shifted grating) and the light and grating fringes remain straight during two-wave coupling. The strength of the recorded grating is proportional to the small parameter a_0 .

The spatial profile $u_i(\tilde{z})$ is strongly affected by the value of the normalized interruption time t_i/t_r , which can be both positive and negative; this profile depends also on the input ratio parameter t_0/t_r . Figure 10 shows the impact of the interruption time for $t_0/t_r=4$. At $t_i/t_r=-10$ (curve 1), when the center of the Gaussian pulse is yet far from the input face, the grating is very weak and its profile is most uniform. For $t_i/t_r=5$ (curve 2), when we are already at the trailing edge of the recording pulse, the grating amplitude is close to its maximum. The spatial profile is much less uniform here; the field concentrates near the output face owing to beam coupling. Further increase of t_i/t_r results in erasure of the grating. This erasure occurs much faster near the input face; correspondingly, the field becomes more and more concentrated near the output face. Note that the output value $u_i(\tilde{d})$ for $t_i/t_r=25$ (when the pulse has almost passed the crystal by the interruption moment) is much larger than it is for $t_i/t_r=-10$. The indicated features underline the role on the nonlinear effects during the pulse recording.

As the second step, we have to solve Eqs. (4) and (5) with the boundary condition for the signal amplitude $a(0, \tilde{t})=0$ and the initial condition for the normalized grating amplitude $u_i=u_i(\tilde{z}, \tilde{t}_i)$; the time \tilde{t} is measured here from the moment of switching the pump on. From Eq. (5) we express u via the amplitude of the signal wave,

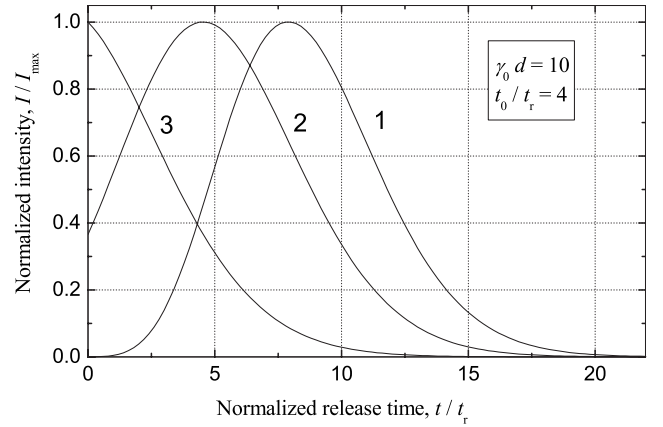


FIG. 11. The normalized output intensity profile I/I_{\max} during the release stage for $t_0/t_r=4$ and $\gamma_0 d=10$. Curves 1, 2, and 3 correspond to $t_i/t_r=-8, 4,$ and $10,$ respectively.

$$u = u_i e^{-\tilde{t}} + \int_0^{\tilde{t}} a(\tilde{z}, \tilde{t}') e^{\tilde{t}' - \tilde{t}} d\tilde{t}'. \quad (15)$$

Substituting this into Eq. (4) we come to the following single integro-differential equation for the auxiliary variable $b = a \exp(\tilde{t})$:

$$\frac{\partial b}{\partial \tilde{z}} = u_i + \int_0^{\tilde{t}} b(\tilde{z}, \tilde{t}') d\tilde{t}'. \quad (16)$$

This equation can be solved by the Laplace transformation. The final result for the normalized amplitude $a=a(\tilde{z}, \tilde{t})$ is

$$a = e^{-\tilde{t}} \int_0^{\tilde{z}} u(\tilde{z}', \tilde{t}_i) I_0\left(2\sqrt{(\tilde{z}-\tilde{z}')\tilde{t}}\right) d\tilde{z}', \quad (17)$$

where $I_0(x)$ is the zero-order modified Bessel function. The structure of the right-hand side resembles that of the expressions describing transient photorefractive processes [31]. It incorporates both the self-enhancement and erasure processes during two-wave coupling. Since $u_i \propto a_0$, the applicability of the undepleted pump approximation during the release stage can be ensured by the use of sufficiently weak signals during recording. The value of a_0 does not influence in this case the shape of the released pulse. With the known explicit expression for $u_i=u(\tilde{z}, \tilde{t}_i)$, given by Eq. (14), we can calculate numerically the output shape of the released pulse.

The impact of the interruption time on the profile of the released pulse is illustrated by Fig. 11. The output profiles are calculated for $t_0/t_r=4$ and $\gamma_0 d=10$. For $t < 0$, i.e., prior to the release process, the signal intensity I is zero. One sees that the shape of the trapped pulse is well reproduced for $t_i/t_r=-8$, when the pulse recording was interrupted at the early stage, curve 1. The half-width of the released pulse, $w/t_r \approx 3.55$, is not much larger than the input width $w_0/t_r \approx 2.35$. Increasing t_i/t_r results in deterioration of the shape of the released pulse, curves 2 and 3. These features are indeed in close connection with the above described impact of the interruption time on the shape of the recorded grating (see Fig. 10).

Note that the number of variable parameters affecting the form of the released pulse is larger compared to the number of input parameters for the pulse deceleration. In addition to the new parameter t_i/t_r , we can consider also the effect of changing pump intensity. Increasing the pump intensity during the release stage leads merely to decrease of t_r and, consequently, to compression of the released pulse.

V. DISCUSSION

The general feature of our theory is the prime role of the photorefractive nonlinearity in achievement of acceptable output characteristics. At small values of the coupling strength, one can speak merely about some signs of pulse deceleration, trapping, and release. At high values of the coupling strength, the spectral properties of the local or nonlocal nonlinear response, although important, are insufficient for judgments about the output characteristics. A thorough analysis of the nonlinear output behavior is indispensable in this range.

Achievement of large values of the coupling strength does not present fundamental difficulties for the PR materials [19,20,22]. At the same time, the range of high nonlinearity is potentially dangerous in view of unwanted parasitic nonlinear effects. The best known of them is the light-induced scattering caused by the spatial amplification of weak seed scattering [20,30]. Generally, the useful and harmful nonlinear effects are controlled by different parameters. Moreover, there are different schemes for optimization of the key output parameters which depend on the type of PR response. This is why an analysis of the capabilities of the main types of PR nonlinearity—local and nonlocal—is important.

While the slowing-down characteristics have common features for the nonlocal and local responses (an almost linear growth of the pulse delay with the coupling strength and significant nonlinear broadening), there are important differences. For the nonlocal response, it is possible to achieve a strong deceleration of light pulses combined with minor shape distortions by using sufficiently broad input pulses and very large values of the coupling strength. The danger of parasitic nonlinear effects is ultimately high in this case. For the local response this scheme is not possible. Instead, it is profitable to optimize the input pulse width, depending on the coupling strength. This scheme leads to a pretty strong deceleration combined with modest shape distortions; the parasitic light-induced scattering is less dangerous in this case. For both types of PR response, it is possible to achieve a substantial pulse deceleration combined with strong shape distortions and a weak danger of the parasitic nonlinear effects.

The impact of pump depletion on the output characteristics is shown to be different for the transmission and reflection coupling geometries. The pump depletion decreases (increases) the delay time for the transmission (reflection)

configuration. This difference is rooted in different forms of the energy conservation law in these cases. In both cases, pump depletion leads to an essential additional broadening of the output pulses and must be considered as a phenomenon to be avoided.

The PR nonlinearity offers ideal possibilities for trapping of light pulses, their long-term storage, and release on demand. They are closely related to the nature of this nonlinearity—the refractive index change is here due to the light-induced space-charge field, which can be frozen for a long time once the light is switched off. The pulse trapping and release represent strongly nonlinear effects, which are affected generally by the characteristics of the recording, storage, and readout stages. The shape of the released pulse sharply depends on the choice of the trapping moment.

Among the advantages of the PR nonlinearity is the possibility to use ambient temperatures, low-power common light sources, and a broad spectral band of extrinsic absorption. Numerous materials with different optical and PR properties are also available. A serious drawback of the PR nonlinearity is its slowness; the response time t_r can be as long as seconds or even minutes in such materials as BaTiO₃ and LiNbO₃ for low-power laser sources. To decrease the response time significantly, it is necessary to switch to the range of high intensity and/or to fast PR crystals, such as Bi₁₂SiO₂₀ or Sn₂P₂S₆ [20,27].

The first experimental data for PR pulse deceleration, which are available in the literature [15,16], are in good agreement with our theory. More efforts, however, are necessary to improve and optimize the output characteristics for particular materials.

VI. CONCLUSIONS

We have developed a theory of photorefractive manipulation of light pulses, including the pulse deceleration, trapping, and release on demand. The key element of this theory is the nonlinear character of the effects in question. The main characteristics of pulse deceleration, including the pulse delay, the output width, and the peak amplification factor, are analyzed in detail for the cases of local and nonlocal photorefractive response. Different schemes of optimization of the output parameters are considered. The impact of the pump depletion on the pulse deceleration is found to be essentially different for the transmission and reflection interaction geometries but harmful in any case. It is shown that the light pulses can be effectively trapped, stored for a long time, and released on demand. The strong impact of the trapping time on the shape of the released pulses is predicted.

ACKNOWLEDGMENT

Financial support from the Russian Foundation for Basic Research (Grant No. 07-02-00301a) is gratefully acknowledged.

- [1] L. V. Hau, S. E. Harris, Z. Dutton, and C. Behroozi, *Nature* (London) **397**, 594 (1999).
- [2] R. W. Boyd and D. J. Gauthier, in *Progress in Optics*, edited by E. Wolf (Elsevier, Amsterdam, 2002), Vol. 43.
- [3] M. S. Bigelow, N. N. Lepeshkin, and R. W. Boyd, *Science* **301**, 200 (2003).
- [4] M. O. Scully and G. R. Welch, *Phys. World.* **17**, 31 (2004).
- [5] R. W. Boyd and P. Narum, *J. Mod. Opt.* **54**, 2403 (2007).
- [6] Y. M. Vlasov, M. O'Boyle, H. F. Hamann, and S. J. McNab, *Nature* (London) **438**, 65 (2005).
- [7] Z. Dutton and L. Vestergaard Hau, *Phys. Rev. A* **70**, 053831 (2004).
- [8] C. Liu, Z. Dutton, C. Behroozi, and L. V. Hau, *Nature* (London) **409**, 490 (2001).
- [9] S. E. Harris, *Phys. Today* **50**, 36 (1997).
- [10] D. F. Phillips, A. Fleischhauer, A. Mair, R. L. Walsworth, and M. D. Lukin, *Phys. Rev. Lett.* **86**, 783 (2001).
- [11] A. V. Turukhin, V. S. Sudarshanam, M. S. Shahriar, J. A. Musser, B. S. Ham, and P. R. Hemmer, *Phys. Rev. Lett.* **88**, 023602 (2002).
- [12] M. S. Bigelow, N. N. Lepeshkin, and R. W. Boyd, *Phys. Rev. Lett.* **90**, 113903 (2003).
- [13] Y. Okawachi, M. S. Bigelow, J. E. Sharping, Z. Zhu, A. Schweinsberg, D. J. Gauthier, R. W. Boyd, and A. L. Gaeta, *Phys. Rev. Lett.* **94**, 153902 (2005).
- [14] A. Schweinsberg, N. N. Lepeshkin, M. S. Bigelow, R. W. Boyd, and S. Jarabo, *Europhys. Lett.* **73**, 218 (2006).
- [15] E. Podivilov, B. Sturman, A. Shumelyuk, and S. Odoulov, *Phys. Rev. Lett.* **91**, 083902 (2003).
- [16] A. Shumelyuk, K. Shcherbin, S. Odoulov, B. Sturman, E. Podivilov, and K. Buse, *Phys. Rev. Lett.* **93**, 243604 (2004).
- [17] G. Zhang, R. Dong, F. Bo, and J. Xu, *Appl. Opt.* **43**, 1167 (2004).
- [18] G. Zhang, F. Bo, R. Dong, and J. Xu, *Phys. Rev. Lett.* **93**, 133903 (2004).
- [19] M. P. Petrov, S. I. Stepanov, and A. V. Khomenko, *Photorefractive Crystals in Coherent Systems* (Springer-Verlag, Berlin, 1991).
- [20] L. Solymar, D. Webb, and A. Grunnet-Jepsen, *The Physics and Applications of Photorefractive Materials* (Clarendon, Oxford, 1996).
- [21] R. W. Boyd, *Nonlinear Optics* (Academic Press, London, NY, 1992).
- [22] *Photorefractive Materials and Their Applications*, edited by P. Günter and J.-P. Huignard (Springer-Verlag, Berlin, 1989).
- [23] A. M. Glass, D. von der Linde, and T. G. Negran, *Appl. Phys. Lett.* **25**, 233 (1974).
- [24] B. I. Sturman and V. M. Fridkin, *The Photovoltaic and Photorefractive Effects in Noncentrosymmetric Crystals* (Gordon and Breach, Philadelphia, 1992).
- [25] J. Mathews and R. L. Walker, *Mathematical Methods of Physics* (W. A. Benjamin, New York, 1964).
- [26] B. I. Sturman, in *Photorefractive Materials and Their Applications*, edited by P. Günter and J. Huignard (Springer, New York, 2006), Vol. 1.
- [27] A. A. Grabar, Yu. M. Vysochanskii, A. N. Shumelyuk, M. Jazbinsek, G. Montemezzani, and P. Günter, in *Photorefractive Materials and Their Applications*, edited by P. Günter and J.-P. Huignard (Springer, New York, 2006), Vol. 2.
- [28] B. Sturman, P. Mathey, H. R. Jauslin, S. Odoulov, and A. Shumelyuk, *J. Opt. Soc. Am. B* **24**, 1303 (2007).
- [29] M. Jeganathan, M. C. Barshaw, and L. Hesselink, *J. Opt. Soc. Am. B* **12**, 1370 (1995).
- [30] B. I. Sturman, S. G. Odoulov, and M. Yu. Goukov, *Phys. Rep.* **275**, 197 (1996).
- [31] Yu. M. Osipov and B. I. Sturman, *Opt. Commun.* **79**, 345 (1990).